Open Journal of Applied Sciences, 2016, 6, 217-233
Published Online April 2016 in SciRes. http://www.scirp.org/journal/ojapps
http://dx.doi.org/10.4236/ojapps.2016.64023

Theoretical Study of Laser Emission for C-Like (Ar XIII), (Ti XVII) and (Fe XXI)

Wessameldin S. Abdelaziz[1], Th. M. El Sherbeni[2], Nahed H. Wahba[1]

[1]National Institute of Laser Enhanced Sciences, Cairo University, Giza, Egypt
[2]Laser and New Materials Laboratory, Physics Department, Faculty of Science, Cairo University, Giza, Egypt
Email: nhew77@yahoo.com, wessamlaser@yahoo.com

Received 7 March 2016; accepted 12 April 2016; published 15 April 2016

Abstract

Energy levels, transition probability and oscillator strengths have been calculated for the Ar XIII, Ti XVII and Fe XXI. The configurations included in the calculations are $2s^2\ 2p^2$, $2s^2\ 2p\ 3l$ (l = s, p & d) and 4l (l = s, p, d, & f) of C-like Ar XIII, Ti XVII & Fe XXI which has 69 fine structures by using the fully relativistic flexible atomic code (FAC) program. These data are used in the determination of the reduced population and gain coefficients over a wide range of electron densities from (10^{+18} to 10^{+23}) and at various plasmas temperatures. The results show that the transitions in Ar^{18+}, Ti^{22+}, and Fe^{26+} ions are the most promising laser emission lines in the XUV and soft X-ray spectral regions.

Keywords

XUV, Soft X-Ray, Laser Radiation, Population Inversion, Gain Coefficient

1. Introduction

The last three decades enormous advances in our understanding and developing high-efficiency of X-ray laser with gain [1] [2] by using the mechanism for demonstrating X-ray lasing in resonant photo pumping have been seen. The pump power needed to achieve inversion was extremely high. (ECP) electron collisional pumping has been the most familiar and suitable pumping mechanisms used in soft X-ray lasers [3]. The modeling of astrophysical and laboratory plasmas used c-like ions and their emission lines. Those data for transition mostly lie in the soft X-ray and EUV regions [4]. Energy levels, spontaneous decay rates and oscillator strengths have been calculated by Aggrawal *et al.* [5] [6], Feldman *et al.* [7] & Aggrawal *et al.* [8] for transitions in Ar XIII, Ti XVII & Fe XXI. But no much work has been done to predict the gain of C-like Ar XIII, Ti XVII & Fe XXI theoretically.

How to cite this paper: Abdelaziz, W.S., El Sherbeni, Th.M. and Wahba, N.H. (2016) Theoretical Study of Laser Emission for C-Like (Ar XIII), (Ti XVII) and (Fe XXI). *Open Journal of Applied Sciences*, **6**, 217-233.
http://dx.doi.org/10.4236/ojapps.2016.64023

In this paper, we calculate energy levels for 69 fine-structure states using a fully relativistic approach based on Dirac equation. Weighted oscillator strengths, spontaneous radiative decay rates are calculated in the single multipole approximation, and collision strengths by electron impact using the factorization-interpolation method are calculated in the distorted wave approximation. Effective collision strengths are calculated by interpolating the data from the collision strengths and integrating over Maxwellian distribution at different temperatures. Rate coefficients are calculated from effective collision strengths using a formula that will be described later in this paper. Then, we predict the reduced population and gain coefficient for C-like Ar XIII, Ti XVII & Fe XXI by a steady state equation in the collisional radiative model after achieving a population inversion between the allowed transition states.

2. Computation of Gain Coefficient

The possibility of laser emission from plasma of Ar XIII, Ti XVII and Fe XXI ions via electron collisional pumping, in the XUV spectral region was investigated at different plasma temperatures and electron densities.

The reduced population densities were calculated by solving the coupled rate equations [7]-[10].

$$N_j\left[\sum_{i<j}A_{ji}+N_e\left(\sum_{i<j}C^d_{ji}+\sum_{i>j}C^e_{ji}\right)\right]=N_e\left(\sum_{i<j}N_iC^e_{ij}+\sum_{i>j}N_iC^d_{ij}\right)+\sum_{i>j}N_iA_{ij}. \tag{1}$$

where N_j and N_i is the fractional population of level $jandi$ respectively, N_e is the electron density, A_{ji} is the Einstein coefficient for spontaneous radiative decay from *j* to *i*; and C^e_{ij} and C^d_{ji} represent the rate coefficient for collisional excitation and de-excitation respectively. The actual population density N_J of the j^{th} level can be calculated from the equation of identity [11] [12].

$$C^d_{ji}=C^e_{ij}\left[\frac{g_i}{g_j}\right]\exp\left[\frac{\Delta E_{ji}}{kT_e}\right]. \tag{2}$$

where g_i and g_j are the statistical weights of the lower and upper levels, respectively.

The electron impact excitation rates usually are expressed via the effective collision strengths γ_{ji} as

$$C^d_{ji}=\frac{8.6287\times10^{-6}}{g_jT_e^{1/2}}\gamma_{ij}. \tag{3}$$

where the values of γ_{ji} and A_{ji} are obtained by [11].

The actual population density N_J of the j^{th} level is obtained from the following identity [11],

$$N_J=N_j*N_i. \tag{4}$$

where N_I is the quantity of ions which reached to the ionization stage I [11],

$$N_I=f_I\,N_e/Z_{avg}\,. \tag{5}$$

where N_e is the electron density, Z_{avg} is the average degree of ionization and f_I is the fractional abundance of the ionization states which can be calculated from the relation [11]. Since the populations density from Equation (1) are normalized such that,

$$\sum_{J=1}^{69}\frac{N_J}{N_I}=1. \tag{6}$$

After the calculation of levels population density, the quantities N_j/g_j and N_i/g_i can be calculated.

Once a population inversion has been ensured a positive gain through $F>0$ [13] is obtained by

$$F=\frac{g_j}{N_j}\left[\frac{N_j}{g_j}-\frac{N_i}{g_i}\right]. \tag{7}$$

where N_j/g_j and N_i/g_i are the reduced populations of the upper level and lower level respectively. Equation (7) has been used to calculate the gain coefficient (α) for Doppler broadening of the various transitions in the Ar XIII, Ti XVII and Fe XXI ion.

$$\alpha_{ji} = \frac{\lambda_{ij}^3}{8\pi}\left[\frac{M}{2\pi K T_i}\right]^{1/2} A_{ji} N_j F \ . \quad (8)$$

where M is the ion mass λ_{ij} is the transition wavelength in (nm), T_i is the ion temperature in K and j, i represent the upper and lower transition levels respectively.

3. Results and Discussions

3.1. Energy Levels

By using the fully relativistic flexible atomic code (FAC) [14] we obtained energy level values for the $1s^2$ $2s^2$ 2pnl (n = 3, l = s, p & d) and ml (m = 4, l = s, p, d & f) configurations in C-like Ar^{18+}, Ti^{22+} and Fe^{26+} ions. This data presented in **Tables 1-3**. The first column of each table provides an index for the levels, the second column presented the main components of the computed eigenvectors and the third column presented our calculations of energy levels. **Tables 4-6** presented the comparing data between our calculations and with the experimental values compiled by NIST. We obtained the agreement between FAC, Bhatia, Seely and Feldman [15] for Ar^{18+}, Ti^{22+} and Fe^{26+} energy levels and with the other experimental energies [16] [17] with the values available at the National Institute of Standards and Technology (NIST) [18] and is within values less than 0.5% for a majority of levels.

3.2. Level Population

The reduced population densities are calculated for 69 fine structure levels arising from $1s^2$ $2s^2$ 2pnl (n = 3, l = s, p & d) and ml (m = 4, l = s, p, d & f) configurations that emit radiation in the XUV and soft X-ray spectral regions. The calculations were performed by solving the coupled rate Equation (1) simultaneously using MATLAB version 7.10.0 (R2010a) computer program. The reduced populations density are calculated as a function of electron densities and plotted at different plasma temperatures for Ar^{18+}, Ti^{22+} and Fe^{26+} ions.

The behavior of level populations density of the various ions (Ar XIII, Ti XVII & Fe XXI) can be explained as follows: in general, at low electron densities the reduced population density is proportional to the electron density, where excitation to an excited state is followed immediately by radiation decay, and collisional mixing of excited levels can be ignored. This result is in agreement with that of Feldman *et al*. [9] [10] [19]. At high population densities (10^{+23}), radiative decay to all levels will be negligible compared to collisional depopulations and all level populations become independent of electron density and are approximately equal. The 10^{+17} electron density shows a peak at before the other levels then decreases to the saturation faster than the other levels, which mean that then on radiative transitions dominant the de-excitation because of its higher energy and fast decay time (see **Figures 1-9**). The population inversion is largest where electron collisional de-excitation rate for the upper level is comparable to radiative decay for this level [9] [19].

3.3. Inversion Factor

Laser amplification will occur only if there is population inversion, or in other words, for positive inversion factor F > 0. In order to work in the XUV and X-ray spectral regions, we have selecting transitions between any two levels producing photons with wavelengths between 5˚ and 100˚A. The electron density at which the population reaches corona equilibrium approximately equals to A/D, where A is the radiative decay rate and D is the collisional de-excitation rate [13]. The population inversion is largest where the electron collisional de-excitation rate for the upper level is comparable to the radiative decay rate for this level.

3.4. Gain Coefficient

As population inversion will be positive in laser medium. Equation (8) has been used to calculate gain coefficient for the Doppler broadening of various transitions in the Ar XIII, Ti XVII & Fe XXI ions. For F > 0 transition having positive inversion with the maximum gain coefficient in cm^{-1}. The maximum gain was calculated and plotted against electron density **Figures 10-18** these short wavelength laser transitions can be produced using plasmas created by optical lasers as the lasing medium.

For Ar XIII, Ti XVII & Fe XXI ions the rates for electron collisional excitation from the $1s^2$ $2s^2$ 2p2 ground

Table 1. State definitions and energy levels for Ar XIII.

Index	State configuration	E (Ryd)	Index	State configuration	E (Ryd)
1	$(2p_0)_0$	0.0000	36	$(2p_{1/2}\ 4p_{1/2})_1$	39.1208
2	$(2p_{1/2}\ 2p_{3/2})_1$	0.0863	37	$(2p_{1/2}\ 4p_{3/2})_1$	39.1971
3	$(2p_2)_2$	0.1971	38	$(2p_{1/2}\ 4p_{3/2})_2$	39.1979
4	$(2p_{1/2}\ 2p_{3/2})_2$	0.7964	39	$(2p_{1/2}\ 4p_{1/2})_0$	39.2726
5	$(2p_0)_0$	1.7559	40	$(2p_{3/2}\ 4p_{3/2})_1$	39.3571
6	$(2p_{1/2}\ 3s_{1/2})_0$	28.6954	41	$(2p_{3/2}\ 4p_{3/2})_3$	39.3577
7	$(2p_{1/2}\ 3s_{1/2})_1$	28.7310	42	$(2p_{3/2}\ 4p_{1/2})_1$	39.4153
8	$(2p_{3/2}\ 3s_{1/2})_2$	28.9021	43	$(2p_{3/2}\ 4p_{1/2})_2$	39.4239
9	$(2p_{3/2}\ 3s_{1/2})_1$	29.0568	44	$(2p_{3/2}\ 4p_{3/2})_2$	39.5122
10	$(2p_{1/2}\ 3p_{1/2})_1$	29.6982	45	$(2p_{1/2}\ 4d_{3/2})_2$	39.5692
11	$(2p_{1/2}\ 3p_{3/2})_1$	29.8393	46	$(2p_{1/2}\ 4d_{5/2})_3$	39.6292
12	$(2p_{1/2}\ 3p_{3/2})_2$	29.8407	47	$(2p_{1/2}\ 4d_{5/2})_2$	39.6359
13	$(2p_{3/2}\ 3p_{3/2})_3$	29.9824	48	$(2p_{3/2}\ 4p_{3/2})_0$	39.6528
14	$(2p_{3/2}\ 3p_{3/2})_1$	30.0471	49	$(2p_{1/2}\ 4d_{3/2})_1$	39.6770
15	$(2p_{1/2}\ 3p_{1/2})_0$	30.1436	50	$(2p_{3/2}\ 4d_{5/2})_4$	39.7816
16	$(2p_{3/2}\ 3p_{1/2})_1$	30.2300	51	$(2p_{3/2}\ 4d_{3/2})_2$	39.7958
17	$(2p_{3/2}\ 3p_{3/2})_2$	30.2815	52	$(2p_{3/2}\ 4d_{5/2})_3$	39.8333
18	$(2p_{3/2}\ 3p_{3/2})_2$	30.5068	53	$(2p_{3/2}\ 4d_{5/2})_3$	39.8489
19	$(2p_{3/2}\ 3p_{3/2})_0$	30.8649	54	$(2p_{1/2}\ 4f_{5/2})_3$	39.8543
20	$(2p_{1/2}\ 3d_{3/2})_2$	30.8916	55	$(2p_{1/2}\ 4f_{7/2})_3$	39.8564
21	$(2p_{1/2}\ 3d_{5/2})_3$	30.9916	56	$(2p_{1/2}\ 4f_{5/2})_2$	39.8588
22	$(2p_{1/2}\ 3d_{5/2})_2$	31.0308	57	$(2p_{3/2}\ 4f_{7/2})_4$	39.8599
23	$(2p_{3/2}\ 3d_{5/2})_4$	31.1088	58	$(2p_{3/2}\ 4d_{5/2})_2$	39.8675
24	$(2p_{1/2}3d_{3/2})_1$	31.1865	59	$(2p_{3/2}\ 4d_{3/2})_1$	39.8728
25	$(2p_{3/2}\ 3d_{5/2})_2$	31.2333	60	$(2p_{3/2}\ 4d_{3/2})_0$	39.9725
26	$(2p_{3/2}\ 3d_{5/2})_3$	31.3092	61	$(2p_{3/2}\ 4d_{3/2})_3$	39.9729
27	$(2p_{3/2}\ 3d_{5/2})_2$	31.3680	62	$(2p_{3/2}\ 4d_{5/2})_1$	40.0424
28	$(2p_{3/2}\ 3d_{3/2})_1$	31.3878	63	$(2p_{3/2}\ 4f_{5/2})_3$	40.0480
29	$(2p_{3/2}\ 3d_{3/2})_0$	31.4006	64	$(2p_{3/2}\ 4f_{7/2})_4$	40.0666
30	$(2p_{3/2}\ 3d_{5/2})_1$	31.7013	65	$(2p_{3/2}\ 4f_{7/2})_3$	40.0699
31	$(2p_{3/2}\ 3d_{3/2})_3$	31.7232	66	$(2p_{3/2}\ 4f_{5/2})_2$	40.0730
32	$(2p_{1/2}\ 4s_{1/2})_0$	38.7071	67	$(2p_{3/2}\ 4f_{7/2})_5$	40.0863
33	$(2p_{1/2}\ 4s_{1/2})_1$	38.7232	68	$(2p_{1/2}\ 4f_{5/2})_4$	40.0962
34	$(2p_{3/2}\ 4s_{1/2})_2$	38.9157	69	$(2p_{3/2}\ 4f_{5/2})_1$	40.1044
35	$(2p_{3/2}\ 4s_{1/2})_1$	38.9593			

Table 2. State definitions and energy levels for (Ti XVII).

Index	State configuration	E (Ryd)	Index	State configuration	E (Ryd)
1	$(2p_0)_0$	0.00000	36	$(2p_{3/2}\ 4s_{1/2})_1$	64.09600
2	$(2p_{1/2}\ 2p_{3/2})_1$	0.25739	37	$(2p_{1/2}\ 4p_{3/2})_1$	64.20341
3	$(2p_{1/2}\ 2p_{3/2})_2$	0.49960	38	$(2p_{1/2}\ 4p_{3/2})_2$	64.21108
4	$(2p_2)_2$	1.29590	39	$(2p_{1/2}\ 4p_{1/2})_0$	64.28125
5	$(2p_0)_0$	2.52631	40	$(2p_{3/2}\ 4p_{3/2})_1$	64.63728
6	$(2p_{1/2}\ 3s_{1/2})_0$	47.04981	41	$(2p_{3/2}\ 4p_{3/2})_3$	64.65238
7	$(2p_{1/2}\ 3s_{1/2})_1$	47.10776	42	$(2p_{1/2}\ 4d_{3/2})_2$	64.68391
8	$(2p_{3/2}\ 3s_{1/2})_2$	47.56540	43	$(2p_{3/2}\ 4p_{1/2})_1$	64.70436
9	$(2p_{3/2}\ 3s_{1/2})_1$	47.74998	44	$(2p_{3/2}\ 4p_{1/2})_2$	64.70480
10	$(2p_{1/2}\ 3p_{1/2})_1$	48.36709	45	$2p_{1/2}\ 4d_{5/2})_2$	64.78619
11	$(2p_{1/2}\ 3p_{3/2})_2$	48.66453	46	$(2p_{1/2}\ 4d_{5/2})_3$	64.78871
12	$(2p_{1/2}\ 3p_{3/2})_1$	48.68153	47	$(2p_{1/2}\ 4d_{5/2})_1$	64.83746
13	$(2p_{1/2}\ 3p_{1/2})_0$	48.98048	48	$(2p_{3/2}\ 4p_{3/2})_2$	64.83899
14	$(2p_{3/2}\ 3p_{1/2})_3$	49.04420	49	$(2p_{3/2}\ 4p_{3/2})_0$	65.01402
15	$(2p_{3/2}\ 3p_{3/2})_1$	49.07589	50	$(2p_{1/2}\ 4f_{5/2})_3$	65.07590
16	$(2p_{3/2}\ 3p_{1/2})_1$	49.26976	51	$(2p_{1/2}\ 4f_{7/2})_3$	65.08855
17	$(2p_{3/2}\ 3p_{1/2})_2$	49.34863	52	$(2p_{1/2}\ 4f_{5/2})_2$	65.08986
18	$(2p_{3/2}\ 3p_{3/2})_2$	49.67836	53	$(2p_{1/2}\ 4f_{7/2})_4$	65.09372
19	$(2p_{1/2}\ 3d_{3/2})_2$	49.97520	54	$(2p_{3/2}\ 4d_{5/2})_4$	65.21515
20	$(2p_{3/2}\ 3p_{3/2})_0$	50.14425	55	$(2p_{3/2}\ 4d_{3/2})_2$	65.22616
21	$(2p_{1/2}\ 3d_{5/2})_3$	50.17995	56	$(2p_{3/2}\ 4d_{3/2})_3$	65.27683
22	$(2p_{1/2}\ 3d_{5/2})_2$	50.24569	57	$(2p_{3/2}\ 4d_{5/2})_2$	65.31674
23	$(2p_{1/2}3d_{3/2})_1$	50.40375	58	$(2p_{3/2}\ 4d_{3/2})_1$	65.32405
24	$(2p_{3/2}\ 3d_{5/2})_4$	50.51640	59	$(2p_{3/2}\ 4d_{3/2})_0$	65.33165
25	$(2p_{3/2}\ 3d_{3/2})_2$	50.61335	60	$(2p_{3/2}\ 4d_{5/2})_3$	65.45453
26	$(2p_{3/2}\ 3d_{5/2})_3$	50.76292	61	$(2p_{3/2}\ 4d_{5/2})_1$	65.46425
27	$(2p_{3/2}\ 3d_{5/2})_2$	50.85373	62	$(2p_{3/2}\ 4f_{5/2})_3$	65.57382
28	$(2p_{3/2}\ 3d_{3/2})_1$	50.87489	63	$(2p_{3/2}\ 4f_{7/2})_4$	65.58393
29	$(2p_{3/2}\ 3d_{3/2})_0$	50.89299	64	$(2p_{3/2}\ 4f_{7/2})_3$	65.60794
30	$(2p_{3/2}\ 3d_{5/2})_1$	51.29161	65	$(2f_{3/2}\ 4f_{5/2})_2$	65.60980
31	$(2p_{3/2}\ 3d_{3/2})_3$	51.30451	66	$(2p_{3/2}\ 4f_{7/2})_5$	65.61924
32	$(2p_{1/2}\ 4s_{1/2})_0$	63.52156	67	$(2p_{3/2}\ 4f_{5/2})_4$	65.63594
33	$(2p_{1/2}\ 4s_{1/2})_1$	63.54415	68	$(2p_{1/2}\ 4f_{5/2})_1$	65.64922
34	$(2p_{1/2}\ 4s_{1/2})_2$	64.04077	69	$(2p_{3/2}\ 4f_{7/2})_2$	65.66365
35	$(2p_{1/2}\ 4p_{1/2})_1$	64.06898			

Table 3. State definitions and energy levels for Fe XXI.

Index	State configuration	E (Ryd)	Index	State configuration	E (Ryd)
1	$(2p_0)_0$	0	36	$(2p_{1/2}\ 4p_{3/2})_2$	95.45197
2	$(2p_{1/2}\ 2p_{3/2})_1$	0.64205	37	$(2p_{1/2}\ 4p_{1/2})_0$	95.48976
3	$(2p_{1/2}\ 2p_{3/2})_2$	1.046974	38	$(2p_{1/2}\ 4s_{1/2})_2$	95.62434
4	$(2p_2)_2$	2.22993	39	$(2p_{3/2}\ 4s_{1/2})_1$	95.69301
5	$(2p_0)_0$	3.725701	40	$(2p_{1/2}\ 4d_{3/2})_2$	96.02775
6	$(2p_{1/2}\ 3s_{1/2})_0$	69.98660	41	$2p_{1/2}\ 4d_{5/2})_2$	96.17432
7	$(2p_{1/2}\ 3s_{1/2})_1$	70.06545	42	$(2p_{1/2}\ 4d_{5/2})_3$	96.18603
8	$(2p_{3/2}\ 3s_{1/2})_2$	71.07260	43	$(2p_{1/2}\ 4d_{3/2})_1$	96.22650
9	$(2p_{3/2}\ 3s_{1/2})_1$	71.28858	44	$(2p_{3/2}\ 4p_{1/2})_1$	96.39314
10	$(2p_{1/2}\ 3p_{1/2})_1$	71.62157	45	$(2p_{3/2}\ 4p_{3/2})_3$	96.43909
11	$(2p_{1/2}\ 3p_{3/2})_2$	72.16925	46	$(2p_{3/2}\ 4p_{1/2})_2$	96.44857
12	$(2p_{1/2}\ 3p_{3/2})_1$	72.18456	47	$(2p_{3/2}\ 4p_{3/2})_1$	96.47588
13	$(2p_{1/2}\ 3p_{1/2})_0$	72.42029	48	$(2p_{1/2}\ 4f_{5/2})_3$	96.53988
14	$(2p_{3/2}\ 3p_{3/2})_1$	73.00730	49	$(2p_{1/2}\ 4f_{5/2})_2$	96.55805
15	$(2p_{3/2}\ 3p_{3/2})_3$	73.02872	50	$(2p_{1/2}\ 4f_{7/2})_3$	96.56406
16	$(2p_{3/2}\ 3p_{1/2})_1$	73.18370	51	$(2p_{1/2}\ 4f_{7/2})_4$	96.56958
17	$(2p_{3/2}\ 3p_{1/2})_2$	73.25095	52	$(2p_{3/2}\ 4p_{3/2})_2$	96.66212
18	$(2p_{1/2}\ 3d_{3/2})_2$	73.72002	53	$(2p_{3/2}\ 4p_{3/2})_0$	96.86913
19	$(2p_{3/2}\ 3p_{3/2})_2$	73.76855	54	$(2p_{3/2}\ 4d_{5/2})_4$	97.14962
20	$(2p_{1/2}\ 3d_{5/2})_3$	74.07187	55	$(2p_{3/2}\ 4d_{3/2})_2$	97.15356
21	$(2p_{1/2}\ 3d_{5/2})_2$	74.12905	56	$(2p_{3/2}\ 4d_{3/2})_3$	97.21578
22	$(2p_{1/2}3d_{3/2})_1$	74.28704	57	$(2p_{3/2}\ 4d_{5/2})_2$	97.27134
23	$(2p_{3/2}\ 3p_{3/2})_0$	74.33629	58	$(2p_{3/2}\ 4d_{3/2})_1$	97.27360
24	$(2p_{3/2}\ 3d_{5/2})_4$	74.86687	59	$(2p_{3/2}\ 4d_{3/2})_0$	97.28356
25	$(2p_{3/2}\ 3d_{3/2})_2$	74.93615	60	$(2p_{3/2}\ 4d_{5/2})_3$	97.43375
26	$(2p_{3/2}\ 3d_{5/2})_3$	75.13969	61	$(2p_{3/2}\ 4d_{5/2})_1$	97.45675
27	$(2p_{3/2}\ 3d_{5/2})_2$	75.27364	62	$(2p_{3/2}\ 4f_{5/2})_1$	97.60659
28	$(2p_{3/2}\ 3d_{3/2})_1$	75.28583	63	$(2p_{3/2}\ 4f_{7/2})_4$	97.62409
29	$(2p_{3/2}\ 3d_{3/2})_0$	75.30911	64	$(2p_{3/2}\ 4f_{5/2})_2$	97.65120
30	$(2p_{3/2}\ 3d_{5/2})_3$	75.80306	65	$(2f_{3/2}\ 4f_{7/2})_3$	97.65434
31	$(2p_{3/2}\ 3d_{5/2})_1$	75.81687	66	$(2p_{3/2}\ 4f_{7/2})_5$	97.67014
32	$(2p_{1/2}\ 4s_{1/2})_0$	94.53285	67	$(2p_{3/2}\ 4f_{5/2})_4$	97.68730
33	$(2p_{1/2}\ 4s_{1/2})_1$	94.56133	68	$(2p_{1/2}\ 4f_{5/2})_1$	97.70366
34	$(2p_{1/2}\ 4p_{1/2})_1$	95.21598	69	$(2p_{3/2}\ 4f_{7/2})_2$	97.72815
35	$(2p_{1/2}\ 4p_{3/2})_1$	95.43674			

Table 4. Comparison between some energy levels for Ar XIII.

Index	NIST[a]	CIV3[b]	S.S[c]	Our calculation[d]
1	0.00000	0.0000	0.00000	0.0000
2	0.89800	0.0878	0.08980	0.0863
3	0.19910	0.1967	0.19910	0.1971
4	0.77468	0.8024	0.77480	0.7964
5	1.47749	1.5421	1.47770	1.7559
6	……	28.6854	28.906	28.6954
7	……	28.7216	28.9412	28.7310
8	28.796	28.8765	29.1048	28.9021
9	28.951	29.0507	29.2566	29.0568
10	…..	29.6469	30.0305	29.6982
11	……	29.7816	29.8938	29.8393
12	…..	29.7993	30.0331	29.8407
13	……	29.9319	30.1695	29.9824
14	……	29.986	30.2343	30.0471
15	……	29.995	30.332	30.1436
16	……	30.0848	30.4146	30.2300
17	…..	30.127	30.4676	30.2815
18	……	30.4584	30.6885	30.5068
19	……	30.8405	31.0955	30.8649
20	……	30.843	31.0453	30.8916
21	30.8965	30.9316	31.1857	30.9916
22	30.9375	30.967	31.2402	31.0308
23	……	31.0421	31.3014	31.1088
24	31.0833	31.1439	31.4116	31.1865
25	31.2291	31.1757	31.4473	31.2333
26	31.2291	31.2535	31.5267	31.3092
27	31.2793	31.3024	31.5779	31.3680
28	31.2905	31.3172	31.5917	31.3878
29	……	31.3272	31.5996	31.4006

Note: (a) NIST [18] data; (b) CIV3 program by K. M. Aggarwal [5] (c) SS. The data from the work done by Bhatia *et al.* [15] & (d) Our calculations calculated by the fully relativistic flexible atomic code (FAC).

state to the $1s^2\ 2s^2\ 2p\ 3l$ (l = s, p, d) configuration are greater than the rates for excitation from the ground state to the $1s^2\ 2s^2\ 2p\ 4l$ state. For electron densities and electron temperatures that are typical of laboratory high-density plasma sources this agreement with Feldman *et al.* [9], such as laser-produced plasmas, it is possible to create a quasi-stationary population inversion in this ion.

Under favorable conditions large laser gains for this transition in the XUV and soft X-ray regions of the spectrum can be achieved in the carbon-like Ar XIII, Ti XVII & Fe XXI ions from our calculation. The gain calculations were performed at various electron temperatures and at various electron densities. It is obvious that the gain increases with the temperature.

Table 5. Comparison between some energy levels for Ti XVII.

Index	NIST[a]	GRASP[b]	S.S[c]	Our calculation[d]
1	0.00000	0.00000	0.0000	0.00000
2	0.27030	0.26830	0.2703	0.25739
3	0.50700	0.50780	0.5078	0.49960
4	1.28170	1.30570	1.2815	1.29590
5	2.20690	2.21410	2.2068	2.52631
6	…..	46.58260	47.3506	47.04981
7	46.87000	46.91220	47.4085	47.10776
8	47.32000	47.35860	47.8460	47.56540
9	47.00000	47.55000	48.0273	47.74998
10	….	48.17220	48.6539	48.36709
11	…..	48.45840	48.9590	48.66453
12	….	48.47080	48.9439	48.68153
13	……	48.64740	49.2571	48.98048
14	…….	48.83170	49.5318	49.04420
15	……	48.84590	49.3079	49.07589
16	…..	48.97240	49.3408	49.26976
17	……	49.02320	49.6155	49.34863
18	…..	49.45670	49.9344	49.67836
19	49.86000	49.84550	50.2686	49.97520
20	…..	49.95410	50.3954	50.14425
21	….	50.04190	50.4673	50.17995
22	50.13000	50.10920	50.5499	50.24569
23	50.29000	50.27270	50.7220	50.40375
24	….	50.37240	50.7902	50.51640
25	50.50000	50.47020	51.1449	50.61335
26	50.63000	50.62200	51.0610	50.76292
27	50.73000	50.70710	50.9052	50.85373
28	…….	50.72240	51.1574	50.87489
29	……	50.73740	51.1671	50.89299

Note: (a) NIST [18] data, (b) GRASP code by K. M. Aggarwal [4] (c) SS. The data from the work done by Bhatia *et al.* [15] & (d) Our calculations calculated by the fully relativistic flexible atomic code (FAC).

The results have suggested the following laser transitions in the Ar XIII, Ti XVII & Fe XXI plasma ions, wavelength, radiative life time of the upper and lower laser levels in the possible laser transitions and maximum gain coefficient at various temperatures presented in **Tables 7-9**, as the most promising laser emission lines in the XUV and soft X-ray spectral regions.

3.5. Radiative Life Time

The lifetimes are determined almost entirely from the allowed and the strong inter combination transitions. The radiative lifetime τ_j of an excited atomic state *j*, is related to the atomic transition probability A_{ji} by:

$$\tau_j = \frac{1}{\sum_i A_{ji}}. \tag{9}$$

where the sum is extended over all the lower states which can be reached from the upper state by radiative decay.

Table 6. Comparison between some energy levels for Fe XXI.

Index	NIST[a]	GRASP[b]	S.S[c]	Our calculation[d]
1	0	0	0	0
2	0.67298	0.6739	0.67299	0.642056
3	1.06940	1.0760	1.06949	1.046974
4	2.22860	2.2480	2.22849	2.229933
5	3.38973	3.3598	3.38953	3.725701
6	…….	70.1287	70.41273	69.98660
7	…..	70.2158	70.49231	70.06545
8	…..	71.1373	71.45348	71.07260
9	……	71.3831	71.66505	71.28858
10	……	71.7442	72.03515	71.62157
11	…..	72.2626	72.58137	72.16925
12	….	72.2897	725.7715	72.18456
13	….	72.4324	72.8231	72.42029
14	…..	72.9948	73.54385	73.00730
15	…..	73.0898	73.38858	73.02872
16	…..	73.1885	73.37150	73.18370
17	…..	73.2258	73.62396	73.25095
18	…..	73.7326	74.11683	73.72002
19	…..	73.8041	74.13650	73.76855
20	…..	74.0806	74.67552	74.07187
21	73.8253	74.1356	74.49025	74.12905
22	73.7944	74.3122	74.56477	74.28704
23	74.177	74.3713	74.73364	74.33629
24	….	74.8093	75.24441	74.86687
25	74.6090	73.8734	75.66779	74.93615
26	74.6783	75.0917	75.53895	75.13969
27	75.00548	75.2135	75.32598	75.27364
28	…..	75.2181	75.66777	75.28583
29	…..	75.2372	75.67733	75.30911

Note: (a) NIST [18] data, (b) GRASP code by K. M. Aggarwal [20] (c) SS. The data from the work done by Bhatia *et al*. [15]. (d) Our calculations calculated by the fully relativistic flexible atomic code (FAC).

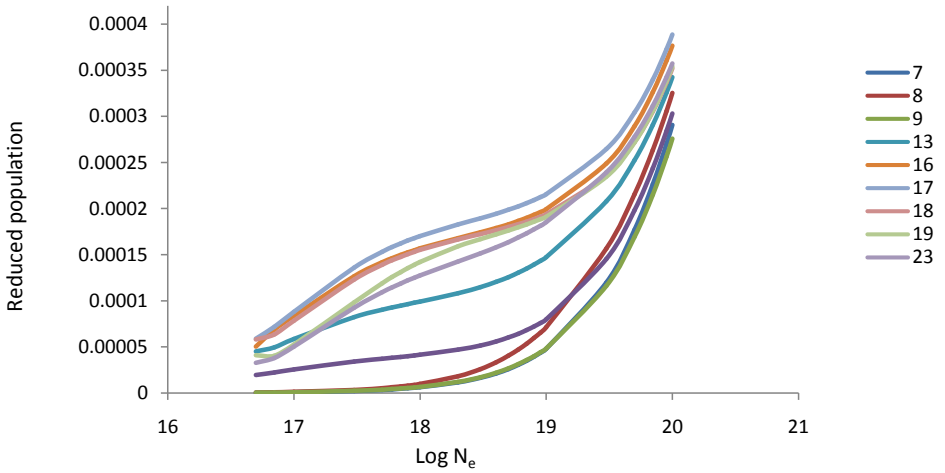

Figure 1. Reduced population of Ar^{+16} levels after electron collisional pumping as a function of the electron density at temperature 300 eV.

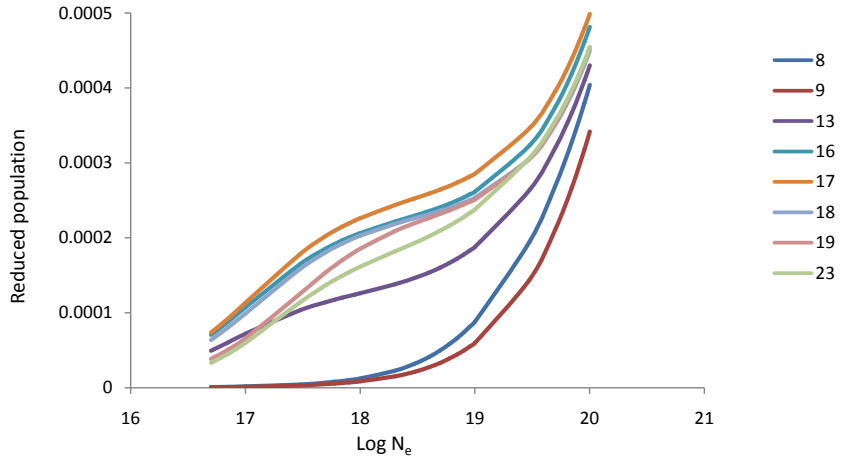

Figure 2. Reduced population of Ar^{+18} levels after electron collisional pumping as a function of the electron density at temperature 400 eV.

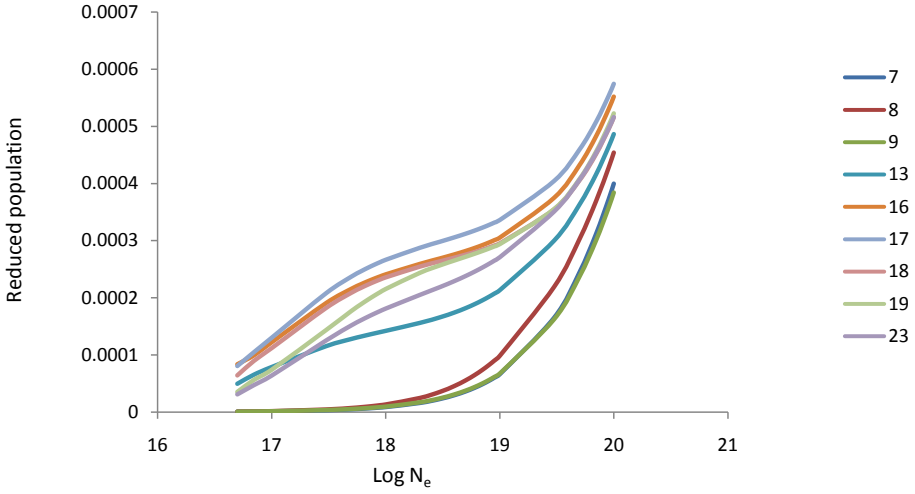

Figure 3. Reduced population of Ar^{+18} levels after electron collisional pumping as a function of the electron density at temperature 500 eV.

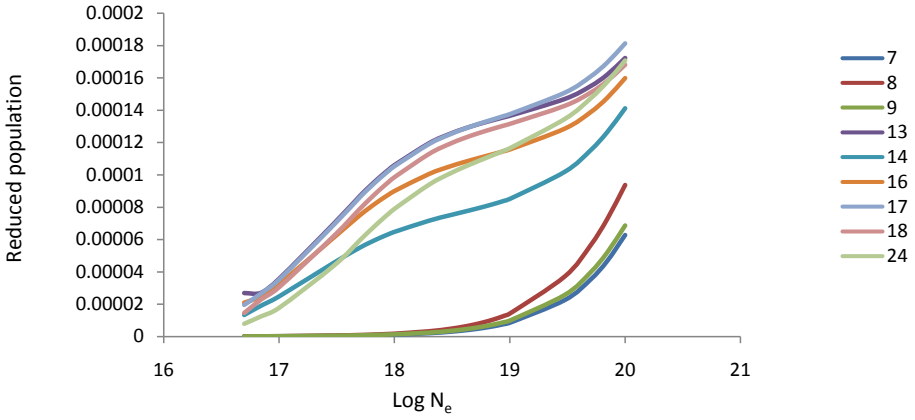

Figure 4. Reduced population of Ti^{+22} levels after electron collisional pumping as a function of the electron density at temperature 400 eV.

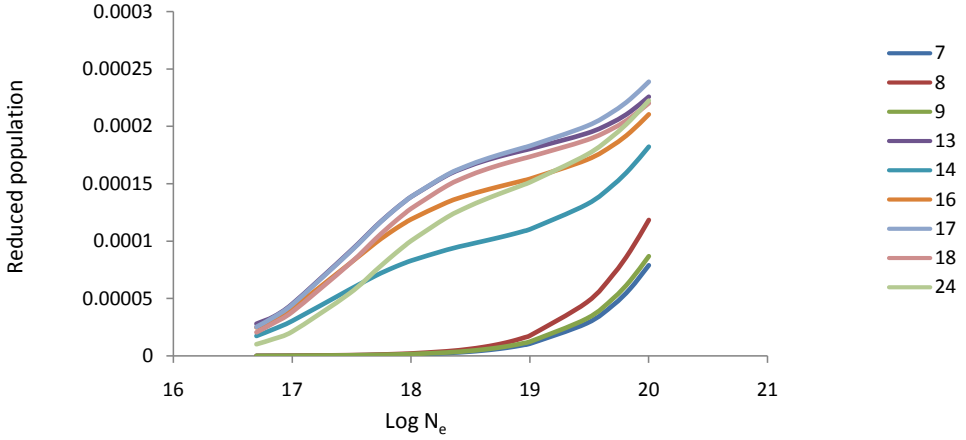

Figure 5. Reduced population of Ti^{+22} levels after electron collisional pumping as a function of the electron density at temperature 500 eV.

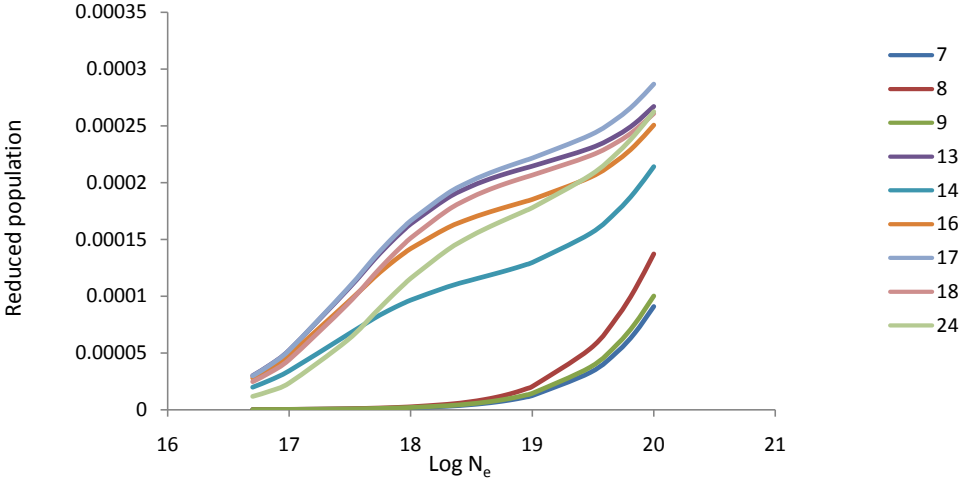

Figure 6. Reduced population of Ti^{+22} levels after electron collisional pumping as a function of the electron density at temperature 600 eV.

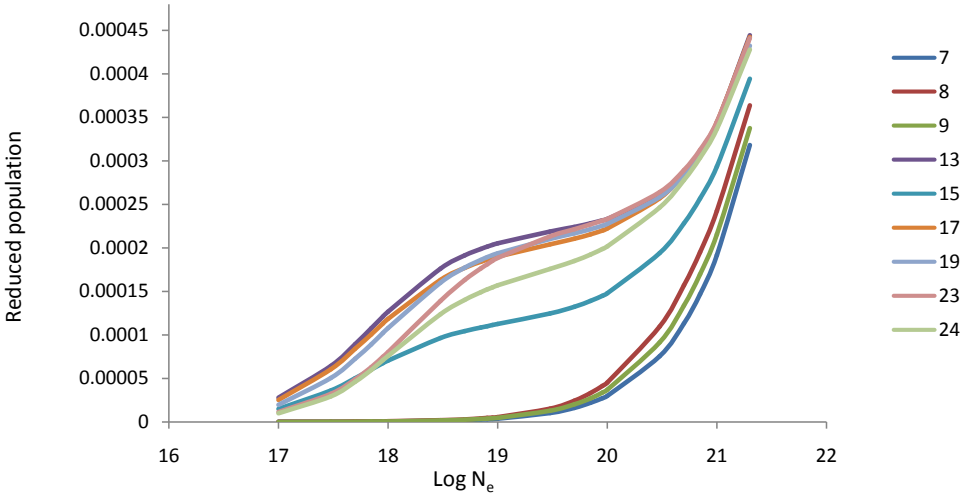

Figure 7. Reduced population of Fe^{+26} levels after electron collisional pumping as a function of the electron density at temperature 900 eV.

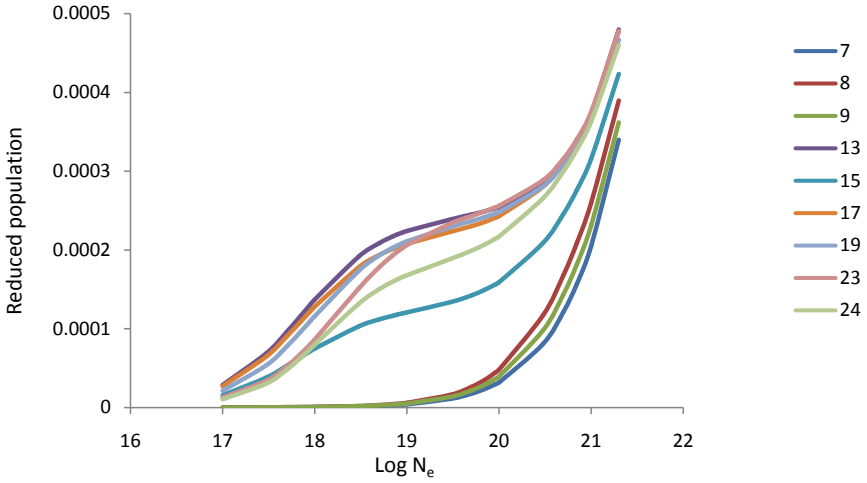

Figure 8. Reduced population of Fe^{+26} levels after electron collisional pumping as a function of the electron density at temperature 1000 eV.

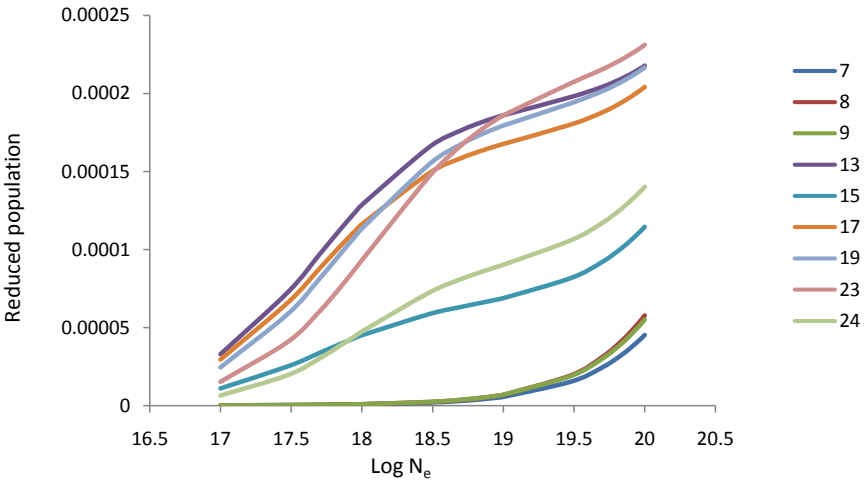

Figure 9. Reduced population of Fe^{+26} levels after electron collisional pumping as a function of the electron density at temperature 1100 eV.

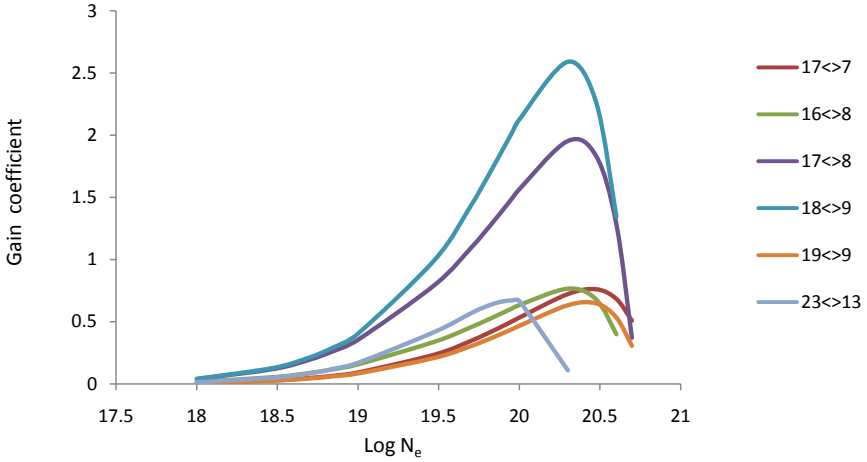

Figure 10. Gain coefficient of possible laser transition against electron density at temperaturev300 eV in Ar^{+18}.

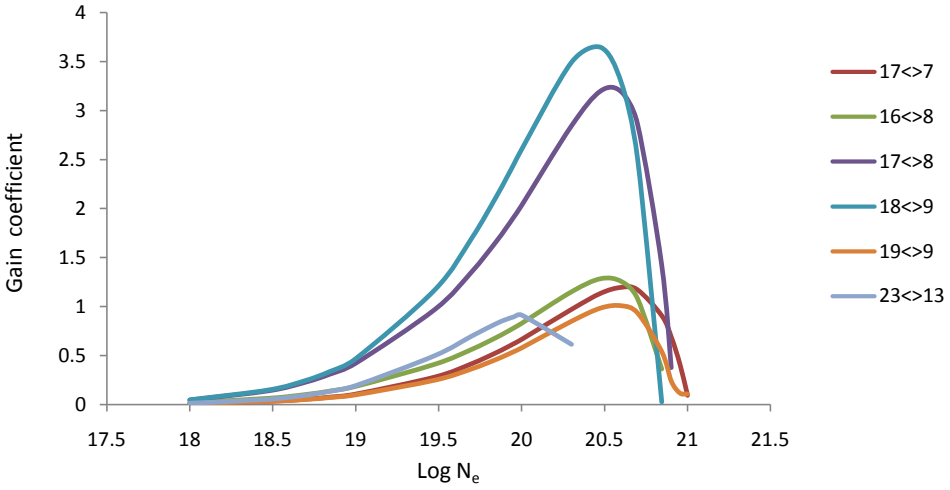

Figure 11. Gain coefficient of possible laser transition against electron density at temperature 400 eV in Ar^{+18}.

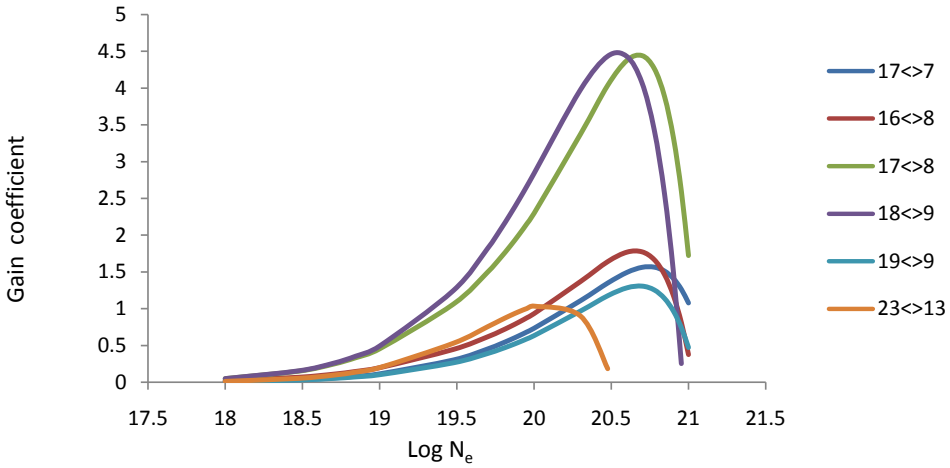

Figure 12. Gain coefficient of possible laser transition against electron density at temperature 500 eV in Ar^{+18}.

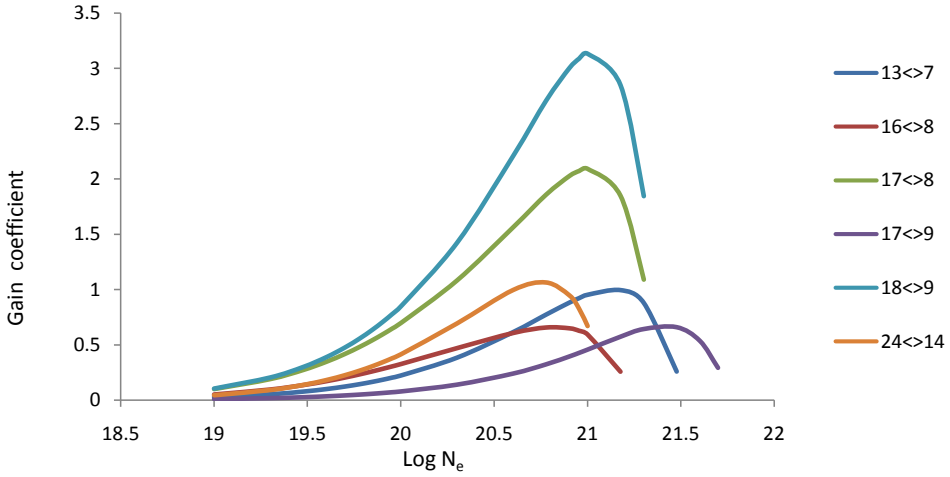

Figure 13. Gain coefficient of possible laser transition against electron density at temperature 400 eV in Ti^{+2}.

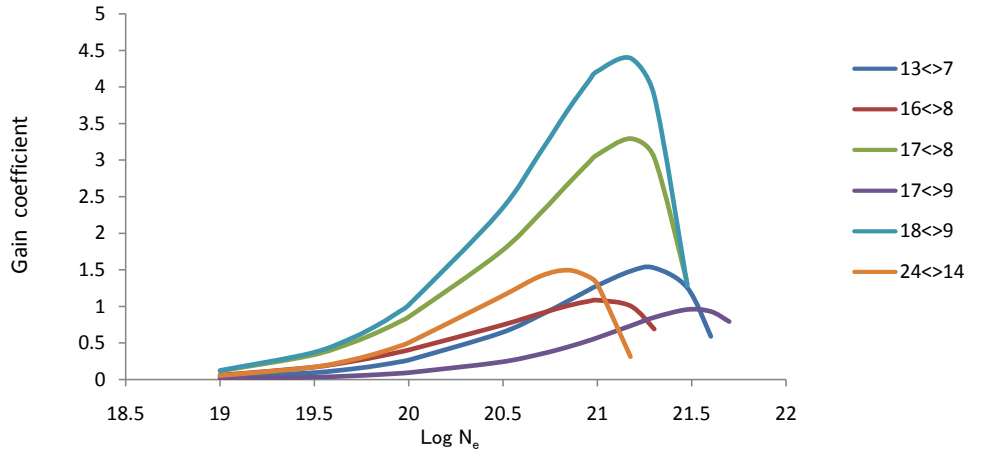

Figure 14. Gain coefficient of possible laser transition against electron density at temperature 500 eV in Ti^{+22}.

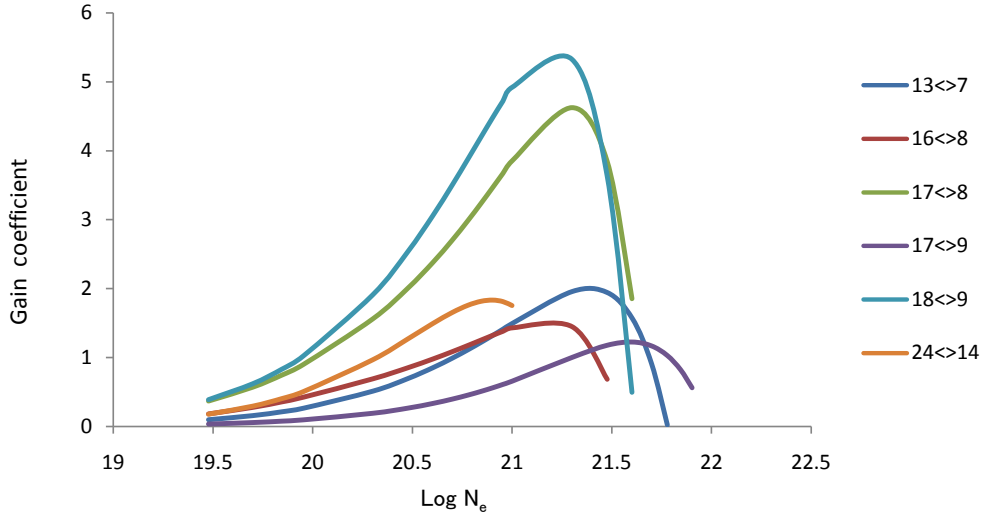

Figure 15. Gain coefficient of possible laser transition against electron density at temperature 600 eV in Ti^{+22}.

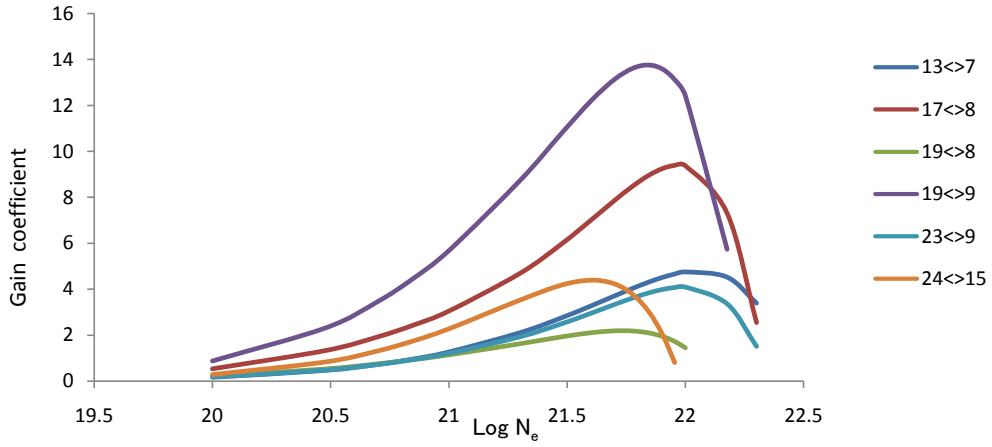

Figure 16. Gain coefficient of possible laser transition against electron density at temperature 900 eV in Fe^{+26}.

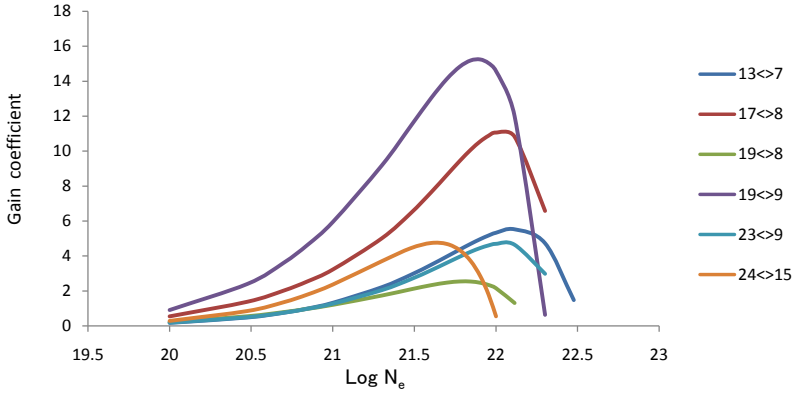

Figure 17. Gain coefficient of possible laser transition against electron density at temperature 1000 eV in Fe^{+26}.

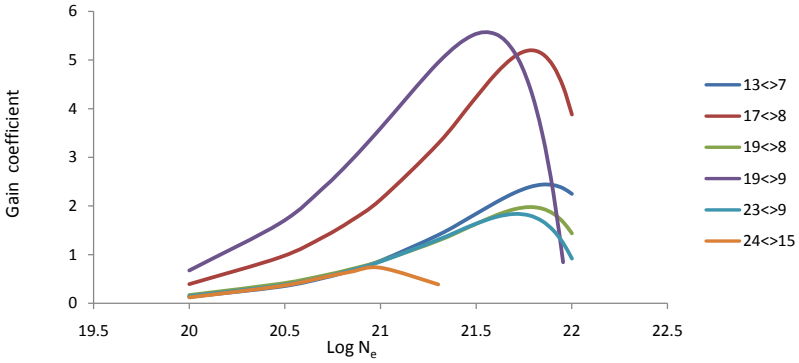

Figure 18. Gain coefficient of possible laser transition against electron density at temperature 1100 eV in Fe^{+26}.

Table 7. Laser transitions, wavelength, radiative life time of the upper and lower laser levels in the possible laser transitions and maximum gain coefficient at temperatures (300, 400 and 500) eV in the possible laser transitions. (Ar XIII)

Transition	Configuration	λ (nm)	τ_j (sec)	τ_j (sec)	Gain (α) (cm^{-1})		
					T = 300 (eV)	T = 400 (eV)	T = 500 (eV)
17<>7	$(2p_{3/2}\ 3p_{3/2})_0$-$(2p_{3/2}\ 3s_{1/2})_1$	49.84	4.47E−10	2.62E−12	0.7607	1.1951	1.5668
16<>8	$(2p_{3/2}\ 3p_{3/2})_2$-$(2p_{1/2}\ 3p_{1/2})_1$	111.4	4.79E−10	1.66E−12	0.7654	1.2835	1.7742
17<>8	$(2p_{1/2}\ 3p_{3/2})_0$-$(2p_{1/2}\ 3p_{1/2})_1$	77.23	4.47E−10	1.66E−12	1.9534	3.1980	4.4397
18<>9	$(2p_{1/2}\ 3d_{3/2})_2$-$(2p_{1/2}\ 3p_{3/2})_1$	56.04	2.25E−10	1.83E−09	2.5906	3.6464	4.4320
19<>9	$(2p_{1/2}\ 3d_{5/2})_3$-$(2p_{1/2}\ 3p_{3/2})_1$	78.21	2.84E−12	1.83E−09	0.6466	1.0078	1.3061
23<>13	$(2p_{1/2}\ 3d_{5/2})_2$-$(2p_{1/2}\ 3p_{1/2})_0$	82.69	2.65E−13	9.34E−10	0.6718	0.9132	1.0337

Table 8. Laser transitions, wavelength, radiative life time of the upper and lower laser levels in the possible laser transitions and maximum gain coefficient at temperatures (400, 500, and 600) eV in the possible laser transitions. (Ti XVII)

Transition	Configuration	λ (nm)	τ_j (sec)	τ_i (sec)	Gain(α) (cm^{-1})		
					T = 400 (eV)	T = 500 (eV)	T = 600 (eV)
13<>7	$(2p_{3/2}\ 3p_{3/2})_1$-$(2p_{3/2}\ 3s_{1/2})_1$	68.0	7.42E−10	1.03E−12	0.9939	1.5261	1.9561
16<>8	$(2p_{3/2}\ 3p_{3/2})_2$-$(2p_{1/2}\ 3p_{1/2})_1$	68.7	3.53E−10	6.74E−13	0.6558	1.0852	1.4478
17<>8	$(2p_{1/2}\ 3d_{3/2})_2$-$(2p_{1/2}\ 3p_{1/2})_1$	56.0	3.04E−10	6.74E−13	2.0915	3.2939	4.6240
17<>9	$(2p_{1/2}\ 3d_{3/2})_2$-$(2p_{1/2}\ 3p_{3/2})_2$	68.8	3.04E−10	9.48E−10	0.6584	0.9560	1.2255
18<>9	$(2p_{3/2}\ 3p_{3/2})_0$-$(2p_{1/2}\ 3p_{3/2})_2$	60.9	1.04E−12	9.48E−10	3.1334	4.3938	5.3260
24<>14	$(2p_{3/2}\ 3d_{5/2})_3$-$(2p_{3/2}\ 3p_{1/2})_1$	60.4	1.58E−13	6.58E−10	1.0624	1.49699	1.8336

Table 9. Laser transitions, wavelength, radiative life time of the upper and lower laser levels in the possible laser transitions and maximum gain coefficient at temperatures (900, 1000 and 1100) eV in the possible laser transitions. (Fe XXI)

Transition	Configuration	λ (nm)	τ_j (sec)	τ_i (sec)	Gain(α) (cm^{-1})		
					T = 900 (eV)	T = 1000 (eV)	T = 1100 (eV)
13<>7	$(2p_{3/2}\,3p_{3/2})_3$-$(2p_{3/2}\,3s_{1/2})_1$	51.8	4.51E−10	4.75E−13	4.7467	5.5314	2.4399
17<>8	$(2p_{3/2}\,3p_{3/2})_2$-$(2p_{1/2}\,3p_{1/2})_1$	42.0	1.04E−12	3.24E−13	9.3873	11.0607	5.1994
19<>8	$(2p_{1/2}\,3d_{5/2})_2$-$(2p_{1/2}\,3p_{1/2})_1$	35.9	1.53E−13	3.24E−13	2.1807	2.5400	1.9796
19<>9	$(2p_{1/2}\,3d_{5/2})_2$-$(2p_{1/2}\,3p_{3/2})_2$	46.0	1.53E−13	9.32E−10	13.7635	15.2395	5.5308
23<>9	$(2p_{3/2}\,3d_{3/2})_2$-$(2p_{1/2}\,3p_{3/2})_2$	32.6	6.82E−10	9.32E−10	4.0888	4.6999	1.8392
24<>15	$(2p_{3/2}\,3d_{5/2})_3$-$(2p_{3/2}\,3p_{1/2})_2$	47.7	8.61E−14	3.60E−10	4.3958	4.7444	0.7326

Tables 7-9 contains the present results of radiative lifetime for the upper and lower laser levels for the (Ar XIII), (Ti XVII) and (Fe XXI).

4. Conclusion

In this work the analysis that has been presented shows that electron collisional pumping (ECP) is suitable for attaining population inversion and offers the potential for laser emission in the spectral region between 30 and 111˚A from the Ar XIII, Ti XVII & Fe XXI ions. This class of lasers can be achieved under the suitable conditions of pumping power as well as electron density. If the positive gains obtained previously for some transitions in the ions under studies (Ar XIII, Ti XVII & Fe XXI ions) together with the calculated parameters could be achieved experimentally, then successful low-cost electron collisional pumping XUV and soft X-ray lasers can be developed for various applications, and the most promising laser emission lines in the XUV and soft X-ray spectral regions.

Acknowledgements

I would like to express my sincere thanks to Mr. Ahmed. Gab Allah for their encouragement and support.

References

[1] Vinogradov, A.V., Sobelmen, I.I. and Yukov, E.A. (1975) Possibility of Constructing Afar-Ultraviolet Laser Utilizing Transitions in Multiply Charged Ions in an Inhomogeneous Plasma. *Soviet Journal of Quantum Electronics*, **5**, 59. http://dx.doi.org/10.1070/QE1975v005n01ABEH010704

[2] Norton, B.A. and Peacock, N.J. (1975) Population Inversion in Laser-Produced Plasmas by Pumping with Opacity-Broadened Lines. *Journal of Physics B*, **8**, 989-996. http://dx.doi.org/10.1088/0022-3700/8/6/026

[3] Eliezer, S. and Mima, K. (2009) Applications of Laser-Plasma Interactions. Taylor & Francis,

[4] Aggarwal, K., Keenan, F. and Msezane, A. (2003) Oscillator Strengths for Transitions in C-Like Ions between KXIV and MnXX. *The Astronomy and Astrophysical Journal*, **401**, 377-383.

[5] Aggarwal, K., Keenan, F. and Msezane, A. (2001) Oscillator Strengths for Transitions in C-Like Ions between FIV and ArXIII. *Journal Supplement*, **136**, 763-787.

[6] Aggarwal, K., Hibbert, A., Keenan, F. and Norrington, P. (1997) Oscillator Strengths for Transitions in CaXV and FeXXI. *Journal of Astrophysical*, **108**, 575-590. http://dx.doi.org/10.1086/312967

[7] Feldman, U., Bhatia, A.K. and Suckewer, S. (1983) Short Wavelength Laser Calculations for Electron Pumping in Ne-Lie Kr (Kr XXVII). *Journal of Applied Physics*, **45**, 2188-2197. http://dx.doi.org/10.1063/1.332371

[8] Feldman, U., Seely, J.F. and Doschek, G.A. (1986) 3S-3P Laser Gain and X-Ray Line Ratios for the Carbon Isoelectronic Sequence. *Journal of Applied Physics*, **59**, 3953-3957. http://dx.doi.org/10.1063/1.336695

[9] Feldman, U., Doschek, G.A., Seely, J.F. and Bhatia, A.K. (1985) Short Wavelength Laser Calculation for Electron Pumping in BeI and BI Isoelectronic Sequences ($18 \leq Z \geq 36$). *Journal of Applied Physics*, **58**, 2909. http://dx.doi.org/10.1063/1.335838

[10] Feldman, U., Seely, J.F. and Bhatia, A.K. (1984) Scaling of Collisional Pumped 3S-3P Lasers in the Neon Isoelectronic Sequence. *Journal of Applied Physics*, **56**, 2475-2478. http://dx.doi.org/10.1063/1.334308

[11] Goldstein, W.H., Oreg, J., Zigler, A. and Klapisch, M. (1988) Gain Prediction for Nickel-Like Gadolinum from a 181-Level Multiconfigurational Distorted-Wave Collisional-Radiative Model. *Physical Review A*, **38**, 1797-1804.

[12] Vinogradov, A.V. and Shleyaptsev, V.N. (1980) Calculation of Population Inversion Due to Transitions in Multiply Charged Neon-Lie Ions in the 200-2000 A Range. *Soviet Journal of Quantum Electron*, **10**, 754. http://dx.doi.org/10.1070/QE1980v010n06ABEH010287

[13] Sobel'man, I.I. (1979) Introduction to the Theory of Atomic Spectra, International Series of Monographs in Natural Philosophy. Vol. 40, Pergamon Press, Oxford.

[14] FAC Code. http://kipac-tree.stanford.edu/fac

[15] Bhatia, A.K., Seely, J.F. and Feldman, U. (1987) Atomic Data and Spectral Line Intensities for the Carbon Iso Electronic Sequence (ArXIII through KrXXXI). *Atomic Data and Nuclear Data Tables*, **36**, 453-494. http://dx.doi.org/10.1016/0092-640X(87)90012-X

[16] Hibbert, A., Ledourneuf, M. and Mohan, M. (1993) Energies, Oscillators Strengths, and Life Times for Neon-Like Ions up to Kr XXVII23-112 ADNDT. *Atomic Data and Nuclear Data Tables*, **53**, 23-112.

[17] Yuan, G., Kato, Y., Daido, H., Kodama, R. and Murai, K. (1996) Accurate Wavelength Determination of the Lasing and Nonlasing Lines in Laser-Produced Germanium Plasma. *Physica Scripta*, **53**, 197-203.

[18] NIST. http://physics.nist.gov/phys Ref Data/ASD/Levels_form.html

[19] Feldman, U., Seely, J.F. and Bhatia, A.K. (1985) Density Sensitive X-Ray Line Ratios in the BeI, BI, and NeI Isoelectronic Sequences. *Journal of Applied Physics*, **58**, 3954-3958. http://dx.doi.org/10.1063/1.335569

[20] Aggarwal, K.M., Hibbert, A., Keenan, F.P. and Norrington, P.H. (1997) Oscillator Strengths for Transitions in Ca_{XV} and Fe_{XXI}. *The Astrophysical Journal Supplement Series*, **108**, 575È590.